JOURNAL OF GUIDANCE, CONTROL, AND DYNAMICS
Vol. 27, No. 6, November–December 2004

Generation of Launch Vehicle Abort Trajectories Using a Hybrid Optimization Method

Anthony J. Calise* and Nico Brandt†
Georgia Institute of Technology, Atlanta, Georgia 30332-0150

Modifications and extensions to a recently developed hybrid numerical–analytical method for optimization of future launch vehicles are presented, to allow for the real time generation of abort trajectories. A set of terminal constraints is formulated that targets an entry condition for the abort case and allows the vehicle to attach tangentially to a nominal entry path. The trajectories are optimal in the sense of maximizing terminal energy. In addition, the algorithm has been extended to include path constraints on both angle of attack and $q \cdot \alpha$. A second issue addressed concerns the possibility of singular arcs, both for nominal ascent and aborts. It is proven that such arcs are not feasible, both within the atmosphere and in vacuum, when the control variables consist of body attitude and throttle. Finally, numerical results for different abort scenarios using a single-stage vehicle model illustrate both the capabilities and some of the deficiencies of the approach.

Nomenclature

A	=	aerodynamic force in axial direction
A_e	=	nozzle exit area
$a_{\max}$	=	maximum axial acceleration
$\boldsymbol{C}$	=	constraint vector
c_e	=	nozzle exit velocity
H	=	Hamiltonian
k	=	constant factor
L	=	thrust independent part of Hamiltonian
M	=	Mach number
m	=	mass
N	=	aerodynamic force in normal direction
$\boldsymbol{P}$	=	velocity costate vector; primer vector
p_a	=	atmospheric pressure
$\boldsymbol{p}_V$	=	collocation variables for velocity state
$\boldsymbol{Q}$	=	position costate vector
q	=	dynamic pressure
$\boldsymbol{q}_R$	=	collocation variables for position costate
$\boldsymbol{q}_V$	=	collocation variables for velocity costate
$\boldsymbol{R}$	=	radius vector from Earth center
R_e	=	Earth radius
S	=	switching function
T	=	thrust
T_{vac}	=	vacuum thrust
$\boldsymbol{V}$	=	inertial velocity vector
α	=	angle of attack
γ	=	flight-path angle
δ	=	angle between primer and body axis
ε	=	constraint multiplier vector
$\boldsymbol{\eta}$	=	vector normal to final orbit plane
θ	=	downrange angle to terminal area energy management (TAEM) point
λ_m	=	mass costate
μ	=	gravitational constant
υ	=	transversality multiplier
ϕ	=	angle between primer and relative velocity
ψ	=	terminal constraint
ω	=	Schuler frequency
$\mathbf{1}_b, \mathbf{1}_d, \mathbf{1}_n$	=	unit vectors along body axis, from Earth center to TAEM point, and perpendicular to body axis
$\mathbf{1}_P, \mathbf{1}_R, \mathbf{1}_V$	=	unit vectors along primer vector, along radius vector, and along velocity vector

Introduction

RELIABLE and affordable access to space, along with a global engagement capability, are now recognized as critical requirements of the U.S. Air Force in the twenty-first century. NASA similarly has established aggressive goals for reduction in both the cost of operations and turnaround time of future reusable launch vehicles and seeks to obtain greatly enhanced safety in operations. Autonomous guidance and control technologies are recognized as critical to the objective of achieving reliable, low-cost, aircraftlike operations into space. Specifically, next-generation systems must be able to fly a variety of vehicle types in multiple mission scenarios, as well as handle dispersions, failures, and abort requirements in a robust fashion.[1]

This paper is concerned with the modifications and extensions to a recently developed hybrid method for launch vehicle trajectory optimization,[2–4] to allow for the real time generation of abort trajectories. There exist a variety of highly developed trajectory optimization codes that use either direct or indirect methods for optimization. However, all of these codes require a reasonably good starting guess for convergence, and most are not suitable for real time guidance application, although a recent example may be an exception.[5] The hybrid method is an attempt to combine analytic and numerical methods to improve the overall solution process in terms of computation effort and reduced sensitivity to an initial guess. The solution process uses an iterative method, which starts from a vacuum solution, and gradually introduces atmospheric effects until a converged solution is obtained. The main advantage of the hybrid approach is that both the trajectory solution and the Jacobian needed for the Newton iteration are nearly analytic. The nonintegrable portions of the equations are treated using the method of collocation. Thus, the analytic portion of the solution becomes the interpolating function used in the collocation solution. Once an atmospheric solution is obtained, updating the solution along the nominal ascent path can be done very quickly using a modern processor. Here we examine use of the hybrid method to generate rapidly an abort trajectory when a failure has occurred; however, the abort formulation is useful for any other method of optimization as well. It is assumed that the nature of the failure is known. We envision that the formulation

Presented as Paper 2002-4560 at the AIAA Guidance, Navigation, and Control, Monterey, CA, 5–8 August 2002; received 31 January 2004; revision received 17 May 2004; accepted for publication 17 May 2004.

*Professor, School of Aerospace Engineering; anthony.calise@ae.gatech.edu. Fellow AIAA.

†Research Visiting Scholar, School of Aerospace Engineering; currently Doctoral Student, Programs and Missions, EADS Astrium GmbH, 88039 Friedrichshafen, Germany; nico.brandt@astrium.eads.net.

can be employed as a follow-up to a method of adaptive guidance for continuing the ascent path before determining the nature of the failure.[6] The focus of this paper is on the formulation of a suitable terminal constraint set defining the entry conditions for the abort case, which is the main extension over previous work[3,4] that did not consider aborts. For this class of problems, it is necessary to account for aerodynamic forces during coast arcs. We do this by treating a coast arc as a zero thrust boost arc with all of the aerodynamic effects accounted for, which is in contrast to previous work[3,4] where coast arcs are treated as purely exoatmospheric arcs. Furthermore, path constraints on both α, $q \cdot \alpha$, and $N(\alpha)$ are modeled, whereas earlier work[3,4] only considered constraints on α and N(α). We also introduce the notion of a q-dependent α constraint to permit greater flexibility in propulsive maneuvering when the dynamic pressure is extremely low. Numerical results for different abort scenarios are presented, and deficiencies with the present approach are discussed. Numerical results are obtained using a vehicle configuration based on X-33 aerodynamic and model data, scaled to represent a larger vehicle capable of attaining a low Earth orbit.

The behavior of the so-called switching function suggests that for single stage (and very likely for two-stage vehicles) the use maximum thrust all along the trajectory is not optimal, even for nominal ascents, giving rise to the issue of the potential optimality of singular arcs. Singular arcs are known to exist in vacuum for two- and three-dimensional rocket trajectories in an inverse-square law gravitational field. These intermediate thrust arcs occur in free-time problems, where there is no upper limit on thrust. The two-dimensional solution is known as Lawden's spiral, due to the form of the trajectory around the center of attraction. Their existence is proven,[7] and numerical solutions containing singular arcs have been presented.[8] However, it has been shown that these solutions are nonoptimal.[9,10] Here we provide a proof that such arcs are not feasible (do not satisfy first-order necessary conditions) both within the atmosphere and in vacuum, when the control variables consist of body attitude and throttle. We further show that throttling using bang–bang control can significantly reduce fuel consumption for single-stage vehicles.

Problem Formulation

The abort guidance problem addressed here is defined for the time period starting at the point where a failure has been identified and assessed and ending where the vehicle reaches an atmospheric entry condition. It is assumed that, at the entry interface, guidance is handed over to a separate algorithm that defines the vehicle trajectory from the entry point to the terminal area energy management (TAEM) point. The total abort maneuver consists of a boost phase and a coast phase, which terminates where it attaches to a nominal entry trajectory. The terminal constraints are written so that the coast trajectory is tangential to the nominal entry trajectory at the attachment point. The duration of the coast phase depends on the location of the TAEM point. Figure 1 shows a typical boost–coast abort trajectory to a downrange TAEM point located sufficiently close to the launch site. Multiple skipping maneuvers occur during the coast phase when the TAEM point is selected far from the launch site, the extreme case being a once-around abort. It is assumed that

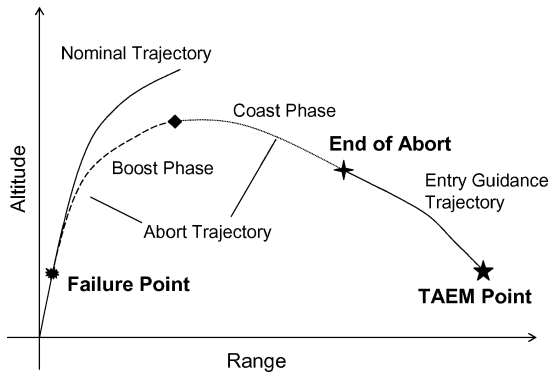

Fig. 1 Abort maneuver and nominal ascent.

final mass is prescribed, so that the final time of the boost phase is determined by the consumption rate of the fuel, which may include any intentional (or accidental) fuel dumping. For example, if the abort is a result of a pump failure (which is the primary failure considered here), then the boost time will depend on the nature of the failure. In any case, the failure, and its effect on thrust and mass flow, are assumed to be known.

State Equations

During burn arcs, the equations of motion for flight in a central gravitational field, expressed in an inertial, Earth-centered coordinate frame are as follows:

$$\begin{bmatrix} \dot{V} \\ \dot{\boldsymbol{R}} \\ \dot{m} \end{bmatrix} = \begin{bmatrix} -\omega^2 \boldsymbol{R} + T_{\text{vac}}/m \cdot \mathbf{1}_P + \boldsymbol{p}_V(t) \\ \boldsymbol{V} \\ -T_{\text{vac}}/C_e \end{bmatrix} \tag{1}$$

where T_{vac} is related to T by $T = T_{\text{vac}} - A_e p_a(\boldsymbol{R})$ and ω is the so-called Schuler frequency defined as

$$\omega = \sqrt{\mu / r_{\text{ref}}^3} \tag{2}$$

In this paper, Earth radius is used as the reference radius magnitude r_{ref}. The vector $\boldsymbol{p}_V(t)$ can be expressed as

$$\boldsymbol{p}_V(t) = \mathbf{1}/m \cdot \{T_{\text{vac}} \cdot (\mathbf{1}_b - \mathbf{1}_P) - [A + A_e p_a(\boldsymbol{R})] \cdot \mathbf{1}_b + N \cdot \mathbf{1}_n\} + \boldsymbol{R} \cdot (\omega^2 - \mu/|R|^3) \tag{3}$$

This vector contains all of the nonlinear aerodynamic effects. These are treated numerically in the hybrid optimization process, using a collocation method. Equations (1–3) can be nondimensionalized. This amounts to letting $\mu = 1$, with the form of the equations remaining otherwise the same.[2] Herein after, all equations will be presented in this nondimensional form (unless otherwise noted), but all numerical results will be presented in dimensional form.

A vacuum solution where the collocation variables are set to zero is generated first.[2] Note from the first element of Eq. (1) that the vacuum solution uses a linear gravity law, which is later corrected by the last term in Eq. (3). It also uses the vacuum optimality condition, $\mathbf{1}_{P_{\text{vac}}} = \mathbf{1}_b$, whereas $\mathbf{1}_P$ in Eq. (3) corresponds to using the full optimality condition (including aerodynamic terms). These approximations permit a nearly analytic solution for the state and costate variables associated within the vacuum solution,[2,11] which in turn allows a nearly analytic Jacobian calculation as well. In a fixed-time formulation, the optimization problem is reduced to solving a set of six nonlinear algebraic equations, which represent a two-point boundary-value problem. The unknowns are the initial position costate and velocity costate values. These are determined so that the constraints and transversality conditions at the final time are met. The collocation variables in Eq. (3), together with those associated with the costate variables (discussed next section), are initially evaluated along the vacuum solution and are introduced in a fixed-point iterative method as an additional forcing term to the solution process. This will of course change the trajectory profile, and so the two-point boundary-value solution is repeated, and the collocation variables are recomputed until the process converges.[2,3]

Coast arcs to be optimized are assumed to occur inside the atmosphere, using the same analytic setup as for burn arcs. Thus, when terminating the abort on a coast arc inside the atmosphere, the aerodynamic effects are accounted for. In an abort maneuver, coast arcs are needed at the end of the trajectory to reach distant TAEM points. However, for abort maneuvers, the endpoint may lie well within the atmosphere. Therefore, the aerodynamic terms may not be negligible for abort trajectories. Because all aerodynamic effects are accounted for on boost arcs, the simplest approach is to treat a coast arc as a zero thrust boost stage. Therefore, boost stages with zero thrust are referred to as atmospheric coast stages, to differentiate them from coast arcs that are treated as purely exoatmospheric arcs.[3,4] If the abort ends on an atmospheric coast stage, final time is determined by enforcing the condition that the Hamiltonian is zero at the final time.

Hamiltonian and Costate Propagation

The Hamiltonian of the system given in Eq. (1) can be expressed in the form

$$H = H_0 + H_{\text{atmos}} + \varepsilon^T \boldsymbol{C}(\boldsymbol{V}, \boldsymbol{R}, \alpha) \tag{4}$$

where

$$H_0 = \boldsymbol{P}^T \cdot \left[-\omega^2 \boldsymbol{R} + T_{\text{vac}} \big/ m \cdot 1_P\right] + \boldsymbol{Q}^T \cdot \boldsymbol{V} - \lambda_m \cdot T_{\text{vac}} / C_e$$

$$H_{\text{atmos}} = \boldsymbol{P}^T \cdot \boldsymbol{p}_V(t) \tag{5}$$

The differential equations for the costates along unconstrained arcs can be written in the following form:

$$\dot{\boldsymbol{P}} = -\boldsymbol{Q} + \boldsymbol{q}_V(t), \qquad \dot{\boldsymbol{Q}} = \omega^2 \boldsymbol{P} - \boldsymbol{q}_R(t) \tag{6a}$$

where

$$\boldsymbol{q}_V(t) = -\frac{\partial H_{\text{atmos}}}{\partial \boldsymbol{V}}, \qquad \boldsymbol{q}_R(t) = \frac{\partial H_{\text{atmos}}}{\partial \boldsymbol{R}} \tag{6b}$$

Performance Index and Terminal Constraints

The objective is to maximize the final velocity magnitude. The performance index is

$$J = k \cdot |\boldsymbol{V}(t_f)| \tag{7}$$

Because final mass is fixed, maximizing the performance in Eq. (7) is equivalent to maximizing the kinetic energy at the end of the abort trajectory ascent. Maximizing terminal velocity can be justified by the operational philosophy that it will maximize the amount of time available for assessing the situation before committing to a course of action. For example, if the attainable velocity for a given landing site (TAEM point) is too high, then one can either delay initiation of the abort maneuver, or dump fuel without burning it. If the attainable velocity is too low, then that landing site can be safely eliminated as an option.

Formulating the terminal constraints for the abort guidance problem is prescribed by the problem of transitioning to entry guidance. There is a good deal of flexibility in defining the entry condition in the abort case with respect to altitude, energy, heading, and position relative to the TAEM point, which in general is referred to as the entry basket. To better address the transition to entry guidance, it is desirable to leave radius and range to the TAEM point open and obtain them as solutions of the optimization process. To achieve this goal, a relation between radius, velocity, and range (longitudinal distance to TAEM point) along the nominal entry path is required. This relation was found by plotting radius and velocity range to the TAEM point for a nominal entry trajectory produced by an entry guidance law.[12]

These plots reveal that along the nominal entry path, radius, and velocity are nearly linear functions of range to the TAEM point, at least over the range of altitudes for which entry guidance is operating. The relation between radius, velocity, and range (represented in terms of the downrange angle θ to the TAEM point) is

$$|\boldsymbol{R}| = K_R \theta R_e + |\boldsymbol{R}_0|$$

$$K_R = 7.5298 \times 10^{-3}, \qquad |\boldsymbol{R}_0| = 2.1013 \times 10^7 \text{ ft}$$

$$|\boldsymbol{V}| = K_V \theta R_e + |\boldsymbol{V}_0|$$

$$K_V = 1.0219 \times 10^{-3} \text{ s}^{-1}, \qquad |\boldsymbol{V}_0| = 2.6965 \times 10^7 \text{ ft/s} \tag{8}$$

where K_R and K_V represent the slope of the linear approximation and $|\boldsymbol{R}_0|$ and $|\boldsymbol{V}_0|$ are the TAEM values. The relation range $= R_e\theta$ is used to simplify the process of calculating the gradients of the terminal constraints used in the buildup of the Jacobian in the hybrid algorithm.[2]

A reasonable set of entry conditions attaching to a nominal entry trajectory is defined by the following conditions:

1) The abort ascent trajectory is tangential to the entry trajectory.

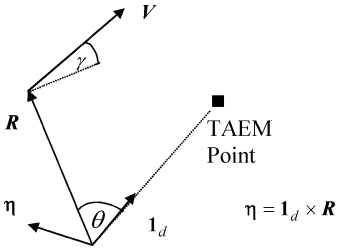

Fig. 2 Terminal constraint vector definitions.

2) A unit vector, $\mathbf{1}_d$, from the Earth center to the TAEM point of the landing site lies in the vehicle's orbit plane as defined by the end of the abort trajectory.

3) The vehicle is flying toward the landing site (not away from it) at the entry interface.

To address the afore-mentioned conditions, the terminal constraints are formulated as follows:

$$\psi_1 = |\boldsymbol{R}| - |\boldsymbol{R}_0| - (K_R/K_V)(|\boldsymbol{V}| - |\boldsymbol{V}_0|) = 0$$

$$\psi_2 = (\mathbf{1}_d \times \mathbf{1}_R)^T [(\mathbf{1}_d \times \mathbf{1}_V)/|\mathbf{1}_d \times \mathbf{1}_V|] + \sin\theta = 0$$

$$\psi_3 = \mathbf{1}_R^T \mathbf{1}_V + C_1 = 0, \qquad \psi_4 = \boldsymbol{V}^T \boldsymbol{\eta} = 0 \tag{9}$$

where

$$\theta = |\boldsymbol{V}| - |\boldsymbol{V}_0|/K_V R_e, \qquad C_1 = K_R \Big/ \sqrt{1 + K_R^2} \tag{10}$$

To obtain the first constraint in Eq. (9), the second expression in Eq. (8) was used to eliminate θ in the first expression in Eq. (8). The second constraint in Eq. (9) ensures that both the constraint on longitudinal distance is met and that condition 3 is satisfied. Note that the vehicle is flying toward the landing site if and only if $\mathbf{1}_d \times \mathbf{1}_V$ points in a direction opposite to that of $\mathbf{1}_d \times \mathbf{1}_R$. The third constraint, on flight-path angle γ, ensures that the vehicle attaches tangential to the entry guidance trajectory, thereby satisfying condition 1. Consequently, the constraint is matched to the altitude and range constraint equations in Eq. (8). This is accomplished by using that altitude, velocity, and range are linked in the vertical plane, which leads to the expression $K_R = \tan\gamma$. The fourth constraint is used to satisfy condition 2, and when it is satisfied, then η is perpendicular to the final orbit plane. See Fig. 2 for a definition of the vectors and their relations.

When the second constraint in Eq. (9) is written, it is assumed that the fourth terminal constraint is simultaneously satisfied. Therefore, these expressions differ from the actual constraints during the solution process and are equivalent to the actual constraints only at the solution point. These simplifications lead to a significant reduction in complexity when deriving the transversality expressions, which involve differentiation of the terminal constraints with respect to the state variables and elimination of the undetermined multipliers associated with each terminal constraint. Moreover, a second differentiation is needed to obtain the expressions necessary to calculate the Jacobian when a Newton method is employed to satisfy these constraints, and the simplifications become even more significant at that stage of the analysis.

To formulate the two-point boundary-value problem, two additional terminal constraints are required. These additional constraints are obtained using the transversality conditions. For the performance index in Eq. (7), the transversality conditions on the costates can be expressed as follows:

$$\boldsymbol{P}(t_f) = \left[k - \upsilon_1(K_R/K_V) + \upsilon_2(\cos\theta/K_V R_e) + \upsilon_3 C_1 |\boldsymbol{R}|\right] \cdot \mathbf{1}_V + \upsilon_2(H_V C_4/|C_3|) - \upsilon_2\left(C_2^T C_3 H_V C_5 \big/ |C_3|^3\right) + \upsilon_3 \boldsymbol{R} + \upsilon_4 \boldsymbol{\eta}$$

$$\boldsymbol{Q}(t_f) = (\upsilon_1 |\boldsymbol{R}| + \upsilon_3 C_1 |\boldsymbol{V}|) \cdot \mathbf{1}_R + \upsilon_2(H_R C_5/|C_3|) + \upsilon_3 \boldsymbol{V} - \upsilon_4(1_d \times V) \tag{11}$$

where

$$C_2 = \mathbf{1}_d \times \mathbf{1}_R, \qquad C_3 = \mathbf{1}_d \times \mathbf{1}_V$$

$$C_4 = -\mathbf{1}_d \times C_2, \qquad C_5 = -\mathbf{1}_d \times C_3$$

$$H_V = \left(I_3 - \mathbf{1}_V \mathbf{1}_V^T\right)\Big/|V|, \qquad H_R = \left(I_3 - \mathbf{1}_R \mathbf{1}_R^T\right)\Big/|\boldsymbol{R}| \quad (12)$$

The unknown multipliers υ_i are eliminated by taking projections of the transversality conditions along $\boldsymbol{\eta}$ and using that $\boldsymbol{\eta}$ is perpendicular to $\boldsymbol{R}$, $\boldsymbol{V}$, C_2, C_3, C_4, and C_5 when the terminal constraint ψ_4 is satisfied. This procedure results in the fifth terminal constraint,

$$\psi_5 = [|\boldsymbol{V}|/|\boldsymbol{R}| \cot\theta \cdot \boldsymbol{P} + \boldsymbol{Q}]^T \boldsymbol{\eta} = 0 \quad (13)$$

For the last constraint, at any time, any single element of $\boldsymbol{P}$ can be set to any value, so long as it has the correct sign. This freedom is because the optimal control is independent of k in Eq. (7). Another way to view this is to recognize that the optimal solution depends only on the orientation of $\boldsymbol{P}$ and not on its magnitude. For simplicity, the first element of the primer vector at the initial time is specified,

$$\psi_6 = \boldsymbol{P}_1(t_0) - 1 = 0 \quad (14)$$

Choosing $\boldsymbol{P}_1(t_0) > 0$ is valid so long as the optimal solution requires that the vertical component of the specific force vector (sum of forces excluding gravity) is positive at the initial time.

When the initial state is assumed to be known, and the initial costate is unknown, then the preceding set of terminal constraints provides the six additional boundary conditions needed to define completely the optimal control solution. For trajectories ending on an atmospheric coast stage, the abort guidance problem is treated as a free-time problem. Then, a seventh constraint can be derived from the condition $H(t_f) = 0$,

$$\psi_7 = -\boldsymbol{P}^T \boldsymbol{R}/|\boldsymbol{R}|^3 + \boldsymbol{Q}^T \boldsymbol{V} = 0 \quad (15)$$

In Eq. (15), the aerodynamic terms in the Hamiltonian have been ignored. These may be significant if transition to entry guidance occurs deep within the atmosphere.

The solution process uses a Newton method with a nearly analytic Jacobian calculation. The information needed for the Jacobian calculation is the gradient of the preceding constraints with respect to the states and costates at the final time.[2] The gradients for Eqs. (9), (13), and (14) are as follows:

$$\boldsymbol{\Psi}_R = \Big[\mathbf{1}_R, H_R C_5/|C_3|, \boldsymbol{V} + |\boldsymbol{V}| C_1 \mathbf{1}_R, -\mathbf{1}_d \times \boldsymbol{V} - \mathbf{1}_d \times (|\boldsymbol{V}|/|\boldsymbol{R}|) \cot\theta \cdot \boldsymbol{P} + \boldsymbol{Q} - (|\boldsymbol{V}|/|\boldsymbol{R}|^2) \cot\theta \cdot \boldsymbol{P}^T \boldsymbol{\eta} \mathbf{1}_R, 0_{3\times 1}\Big]^T$$

$$\boldsymbol{\Psi}_V = \Big[-(K_R/K_V)\mathbf{1}_V, (H_V C_4/|C_3|) - C_2^T C_3 H_V C_5\Big/|C_3|^3 + (\cos\theta/K_V R_e)\mathbf{1}_V$$

$$\boldsymbol{R} + |\boldsymbol{R}| C_1 \mathbf{1}_V, \boldsymbol{\eta}, \left(\boldsymbol{P}^T \boldsymbol{\eta} \mathbf{1}_V \Big/ |\boldsymbol{R}|\right) \cot\theta - |\boldsymbol{V}|\Big/ K_V R_e \sin^2\theta, 0_{3\times 1}\Big]^T$$

$$\boldsymbol{\Psi}_Q = [0_{3\times 4}, \boldsymbol{\eta}, 0_{3\times 1}]^T$$

$$\boldsymbol{\Psi}_P = [0_{3\times 4}, (|\boldsymbol{V}|/|\boldsymbol{R}| \cot\theta \cdot \boldsymbol{\eta}, 0_{3\times 1}]^T \quad (16)$$

The gradient of the Hamiltonian at final time with respect to the states and costates is defined using

$$\boldsymbol{U}^T = [\boldsymbol{R}^T, \boldsymbol{V}^T, \boldsymbol{P}^T, \boldsymbol{Q}^T] \quad (17)$$

Then

$$\boldsymbol{H}_u = \left\{\left[-\boldsymbol{P}/|\boldsymbol{R}|^3 + (3\boldsymbol{P}^T\boldsymbol{R}/|\boldsymbol{R}|^4)1_R\right]^T, \boldsymbol{Q}^T, [-\boldsymbol{R}/|\boldsymbol{R}|^3]^T, \boldsymbol{V}^T\right\} \quad (18)$$

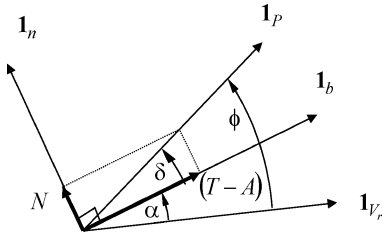

Fig. 3 Optimal control within the atmosphere.

Optimal Control and Feasibility of Singular Arcs

For burn arcs in a vacuum, the control optimality condition reduces to $\mathbf{1}_b = \mathbf{1}_P$, which is a well-known result in the classical literature stating that the propulsive force should be aligned with the primer vector. For the atmospheric part of the trajectory, the control dependent part of the Hamiltonian can be expressed as

$$H(\mathbf{1}_b) = (|\boldsymbol{P}|/m)\Big[(T - A) \cdot \mathbf{1}_P^T \mathbf{1}_b + N \cdot \mathbf{1}_P^T \mathbf{1}_n\Big] + \varepsilon^T \boldsymbol{C}(\boldsymbol{V}, \boldsymbol{R}, \alpha) \quad (19)$$

where both A and N depend on $\mathbf{1}_b$ through the explicit dependence on α. With reference to Fig. 3, the inner products in Eq. (19) can be replaced by the expressions

$$\mathbf{1}_P^T \mathbf{1}_b = \cos\delta, \qquad \mathbf{1}_P^T \mathbf{1}_n = \sin\delta \quad (20)$$

where $\alpha = \phi - \delta$.

Therefore, the control optimality condition reduces to maximizing Eq. (19) with respect to α or δ. A unique maximum occurs when the body axis lies in the plane defined by the primer vector and the velocity vector relative to the atmosphere and is oriented in this plane such that the net force vector (aerodynamic plus propulsive) is nearly aligned with the primer vector. The expressions used to compute $\mathbf{1}_b$ have been previously reported.[3]

When optimal rocket trajectories that include throttling, or thrust control, are dealt with a switching function is used to determine the optimal thrust control policy. The switching function behavior for most of the rocket trajectories generated in this study (nominal ascents and aborts), indicates that using maximum thrust all along the trajectory is not optimal, and either a coast arc or singular arc, or both, should be inserted. In this section, the possibility of a singular arc is examined. Although it has previously been shown that singular arcs are not optimal in a vacuum,[9,10] no references were found in the literature that exclude the possibility of singular arcs within the atmosphere. A proof that such arcs are not feasible is provided here.

The control variables are represented by the orientation of the body/thrust axis $\mathbf{1}_b$ and the vacuum thrust T_{vac}. These control variables are coupled by the optimality condition that the Hamiltonian is maximized with respect to $\mathbf{1}_b$, equivalently represented by the angle δ in Fig. 3. The optimality condition requires that the net force vector is nearly aligned with the primer vector $\mathbf{1}_P$, unless a limit on α [or $q\alpha$ or $N(\alpha)$] is encountered, in which case the solution lies on the limit.

Theorem: Consider the optimal control problem formulation consisting of the dynamics given in Eqs. (1–3) and the performance index given in Eq. (7), subject to a set of control-dependent path constraints. If the vehicle is constrained to fly with positive angle of attack, then singular arcs are not feasible.

Proof: Along an optimal ascent trajectory for which the final time is open, the Hamiltonian can be expressed as

$$H = ST_{\text{vac}} + L + \varepsilon^T \boldsymbol{C}(\boldsymbol{V}, \boldsymbol{R}, \alpha) \quad (21)$$

where

$$S = (|\boldsymbol{P}| \cos\delta/m) - (\lambda_m/c_e)$$

$$L = |\boldsymbol{P}|\left\{[-A - A_e p_a(\boldsymbol{R})/m] \cos\delta + (N/m)\sin\delta - (\mu/|\boldsymbol{R}|^3)\mathbf{1}_b^T \boldsymbol{R}\right\} + \boldsymbol{Q}^T \boldsymbol{V} \quad (22)$$

The constraint terms in Eq. (21) are zero regardless of whether or not the constraint is active. The quantity S is known as the switching function. When $S > 0$, the throttle setting should be maximum, $T_{\text{vac}} = \bar{T}_{\text{vac}}$, and when $S < 0$, the throttle should be at a minimum setting, $T_{\text{vac}} = \underline{T}_{\text{vac}} \geq 0$. Singular arcs are characterized by intermediate throttle settings, along which the solution satisfies

$$S(\delta) = 0 \tag{23}$$

When Eqs. (21) and (23) are combined, it follows that

$$L(\delta) = 0 \tag{24}$$

along a singular arc. [using Eq. (24) instead of Eq. (23) avoids the need to calculate the mass costate λ_m in Eq. (21).] Because body attitude is a control variable, the optimality condition for $\mathbf{1}_b$ also must be satisfied. This first-order necessary condition can be expressed as

$$\frac{\partial H}{\partial \delta} = |\boldsymbol{P}|\left[\left(-T_{\text{vac}} + A_e \cdot p_a(\boldsymbol{R}) + A - \frac{\partial N}{\partial \alpha}\right) \cdot \sin\delta + \left(N + \frac{\partial A}{\partial \alpha}\right) \cdot \cos\delta\right] + \frac{\partial}{\partial \delta}(\varepsilon^T \boldsymbol{C}) = 0 \tag{25}$$

The last term in Eq. (25) is zero when none of the constraints are active. Along a singular arc, the conditions in Eqs. (24) and (25) determine the control variables T_{vac} and $\mathbf{1}_b$ and maintain the stationary condition $[S(t) = 0]$ along the arc. This is represented by the following implied relations:

$$\left.\begin{aligned} &S(\delta) = 0 \Rightarrow L(\delta) = 0 \Rightarrow \delta_s \\ &H_\delta(T_{\text{vac}}, \delta) = 0 \Rightarrow \delta^*(T_{\text{vac}}) \end{aligned}\right\} \Rightarrow T_{\text{vac}_s}(\delta_s) \tag{26}$$

where T_{vac_s} and δ_s are the control solution along a singular arc and $\delta^*(T_{\text{vac}})$ is the solution obtained using the optimality condition in Eq. (25) for any value of $T_{\text{vac}} \geq 0$. In vacuum, $\delta^*(T_{\text{vac}}) = 0$ when $T_{\text{vac}} > 0$.

A singular arc is feasible if and only if $\underline{T}_{\text{vac}} < T_{\text{vac}_s}(\delta_s) < \bar{T}_{\text{vac}}$ for a finite period of time. From the form of Eq. (25), this implies that along a singular arc, $H_\delta(T_{\text{vac}}, \delta_s) < 0$ for all $T_{\text{vac}} > T_{\text{vac}_s}$. Because we are maximizing H, this means that $\delta_s > \delta^*(T_{\text{vac}})$, as shown in Fig. 4.

Figure 4 shows the situation in which there are no active constraints. When a constraint is active, the values of δ^* and δ_s shift to the right. Note from Fig. 3 that $\delta = \phi - \alpha$, where ϕ is held constant when applying the optimality condition. Therefore, when a constraint is active, it follows that $\alpha = \bar{\alpha} < \alpha^*$, which corresponds to $\delta = \underline{\delta} > \delta^*$. It can be seen from Eq. (25) and Fig. 3 that $\delta^*(T_{\text{vac}})$ is a monotonically decreasing function of T_{vac}. Hence, it is impossible to achieve the condition $\delta^*(T_{\text{vac}_s}) = \delta_s$ by decreasing T_{vac}. Consequently, singular arcs are not feasible within the atmosphere.

To address the vacuum condition within the setting of the preceding proof, we examine the expressions in Eq. (26) in the limit $q \to 0$. When Eq. (24) is expanded in a Taylor series up to the second order around $\delta = q = 0$,

$$L(\delta, q) = L(0,0) + \left.\frac{\partial L}{\partial \delta}\right|_0 \delta + \left.\frac{\partial L}{\partial q}\right|_0 q + \left.\frac{\partial^2 L}{\partial q \partial \delta}\right|_0 \delta q + \left.\frac{\partial^2 L}{\partial \delta^2}\right|_0 \frac{\delta^2}{2} + \left.\frac{\partial^2 L}{\partial q^2}\right|_0 \frac{q^2}{2} \tag{27}$$

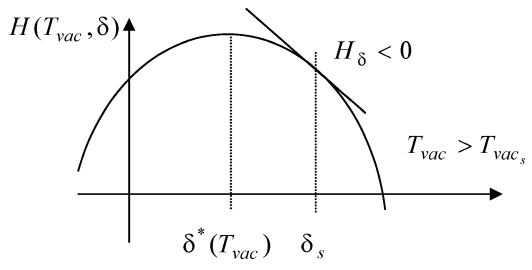

Fig. 4 Hamiltonian vs δ.

where

$$L(0,0) = -|\boldsymbol{P}| \cdot \frac{\mu}{(\boldsymbol{R})^3} \cdot \mathbf{1}_b^T \boldsymbol{R} + \boldsymbol{Q}^T \boldsymbol{V}$$

$$\left.\frac{\partial L}{\partial \delta}\right|_0 = \left.\frac{\partial^2 L}{\partial \delta^2}\right|_0 = \left.\frac{\partial^2 L}{\partial q^2}\right|_0 = 0$$

$$\left.\frac{\partial L}{\partial q}\right|_0 = -|\boldsymbol{P}|\frac{C_A S}{m} \qquad \left.\frac{\partial^2 L}{\partial q \partial \delta}\right|_0 = \frac{|\boldsymbol{P}|}{m}\left[C_N S - C_{A_\delta} S\right] \tag{28}$$

Solving Eq. (27) for δ results in

$$\delta = -L(0,0) - \frac{\partial L}{\partial q} q \Big/ \frac{\partial^2 L}{\partial q \partial \delta} q \tag{29}$$

Note that in Eq. (29) δ is finite for $q \to 0$ if and only if $L(0,0) = 0$. In this case, δ approaches some nonzero value, which contradicts the vacuum optimality condition requiring that $\delta = 0$ □

Remarks: Equation (1) ignores that a component of thrust normal to the x-body axis is required for trim. For example, the shuttle's main engines are canted, resulting in a significant z-body axis component of thrust. However, this approximation does not significantly impact the preceding analysis. For example, if it is assumed instead that the component of thrust along the z-body axis is a linear function of δ, the switching function becomes

$$S = (|\boldsymbol{P}|/m)[\cos\delta + (T_{z_0} + k_z\delta)\sin\delta] - (\lambda_m/c_e) \tag{30}$$

and Eq. (25) can be expressed as

$$\frac{\partial H}{\partial \delta} = |\boldsymbol{P}|\left[\left(-T_{\text{vac}}(1 - k_z) + A_e \cdot p_a(\boldsymbol{R}) + A - \frac{\partial N}{\partial \alpha}\right)\sin\delta + \left(N + T_{z_0} + k_z\delta + \frac{\partial A}{\partial \alpha}\right)\cos\delta\right] + \frac{\partial}{\partial \delta}(\varepsilon^T \boldsymbol{C}) = 0 \tag{31}$$

It can be seen from Eq. (31) that the arguments leading to the conclusion that singular arcs are not feasible remain valid so long as $k_z < 1$. The shuttle is also flown at negative α, which violates the main assumption in the theorem. However, the arguments leading to the conclusion that singular arcs are not feasible could just as easily been phrased with the assumption $\alpha < 0$. Finally, if a constraint (or a combination of constraints) together with the optimality condition imposes a limit on T_{vac}, then the potentially singular control can be viewed as having been eliminated by the constraint. For example, if an axial acceleration limit is active, then $T_{\text{vac}} = m \cdot a_{\max}$. If a purely state-dependent constraint is active, then the constraint is differentiated with respect to time until one or a combination of the control variables appears, and one of the control variables may be viewed as having been eliminated by the constraint. For example, if a dynamic pressure constraint is active, both T_{vac} and α (respectively, δ) appear in the first derivative, so that the constraint can be used to eliminate T_{vac} as a control variable, and the problem becomes regular with respect to $\mathbf{1}_b$.

It can be concluded from the theorem and the preceding remarks that singular arcs are not feasible both within the atmosphere and in vacuum for virtually every circumstance that might be encountered in any practical application. Therefore, if the switching function behavior indicates that using maximum thrust is not optimal, it follows that the solutions should be optimized with respect to throttle control by adding one or more coast arcs.

Path Constraints

The axial acceleration limit is approximated[2] by the condition $T_{\text{vac}}/m \leq a_{\max}$. This assumes that thrust is always dominant over other specific forces, which is perfectly valid outside the atmosphere. Within the atmosphere, it is a conservative approximation and assures that axial acceleration asymptotically approaches its limit as the vehicle exits the atmosphere. The axial acceleration limit is enforced in the optimization process by regulating the mass flow.

The necessary conditions for enforcing angle of attack and $q \cdot \alpha$ limits are summarized in this section. The angle-of-attack limit is modeled as a function of dynamic pressure, so that it can be increased for very low ranges of q to enhance fuel depletion and thrust maneuvering in the upper atmosphere. Angle of attack is treated as a nonnegative quantity in the optimization algorithm under the assumption that the vehicle can be rolled to ensure that this condition is always satisfied. The alpha limit is expressed as

$$|\alpha| \leq \alpha_{\max}(q) \tag{32}$$

When the optimality condition ignoring the limit seeks a solution for α beyond the limit, α is set equal to the limit, and the associated constraint multiplier ε_α is determined from the condition

$$H_\alpha = \frac{\partial H}{\partial \alpha} + \varepsilon_\alpha = 0 \tag{33}$$

where H is the expression for the Hamiltonian without adjoining the constraint term. The corresponding expressions for the costate derivatives along a constraint arc are

$$\dot{\boldsymbol{P}} = -\frac{\partial H}{\partial \boldsymbol{V}} - \varepsilon_\alpha \frac{\partial[\alpha - \alpha_{\max}(q)]}{\partial \boldsymbol{V}}$$

$$\dot{\boldsymbol{Q}} = -\frac{\partial H}{\partial \boldsymbol{R}} - \varepsilon_\alpha \frac{\partial[\alpha - \alpha_{\max}(q)]}{\partial \boldsymbol{R}} \tag{34}$$

Note that it is necessary to eliminate both α and $\alpha_{\max}(q)$ in Eq. (34) because the actual control variable in this formulation is body attitude and not α.

The q-dependent α limit is modeled as a constant for $q > 50$ psf and then is allowed to linearly increase up to 90 deg for the range $50 > q > 3$ psf. For values $q < 3$ psf,the vacuum optimality condition using H_0 is applied to determine the optimal body attitude without a limit on α.

The $q \cdot \alpha$ limit is implemented in a manner identical to that described for the α limit. The only difference lies in that when enforcing both constraints it is necessary to determine the active constraint as the one that results in the lower limit on α. The corresponding expressions needed to compute the constraint multiplier $\varepsilon_{q\alpha}$ and the costate derivatives when the $q \cdot \alpha$ limit is active are

$$H_\alpha = \frac{\partial H}{\partial \alpha} + \varepsilon_{q\alpha} \cdot q = 0, \qquad \dot{\boldsymbol{P}} = -\frac{\partial H}{\partial \boldsymbol{V}} - \varepsilon_{q\alpha} \frac{\partial (q\alpha)}{\partial \boldsymbol{V}} \tag{35}$$

$$\dot{\boldsymbol{Q}} = -\frac{\partial H}{\partial \boldsymbol{R}} - \varepsilon_{q\alpha} \frac{\partial (q\alpha)}{\partial \boldsymbol{R}} \tag{36}$$

The $q \cdot \alpha$ limit leads to convergence problems in some of the abort cases. This problem was addressed by first obtaining the solution without this limit enforced and then enforcing the limit.

Numerical Results

To evaluate the performance of the hybrid approach in optimizing abort trajectories, two different abort scenarios are presented. First, solutions for aborts to TAEM points downrange from the abort condition are shown. Then solutions for an abort resulting in a turn back to the launch longitude are shown. In these results, a fuel pump failure leading to a 30% loss of thrust is modeled. The failure occurs at a point in the nominal ascent profile corresponding to maximum dynamic pressure. After the failure, maximum available thrust is used until the fuel is consumed.

The trajectories are displayed in the launch frame, which is an up–east–north Earth-centered frame, with the up axis passing through the launch site. The nominal ascent profile (100-nmile circular orbit, no failure) is shown as a solid line in all of the results as a point of reference. The $q \cdot \alpha$ limit is set to 2500 lb $\cdot$ deg/ft^2. The q-independent part of the α limit is set to 28 deg. The α and $q \cdot \alpha$ boundaries are shown in Fig. 5. The dashed line indicates a q-dependent linear increase of the α limit until the vacuum optimality condition is used, where no limit is applied. This was introduced to allow greater propulsive maneuvering in regions where the dynamic pressure is very low. Axial acceleration is constrained to 3 g. As shown

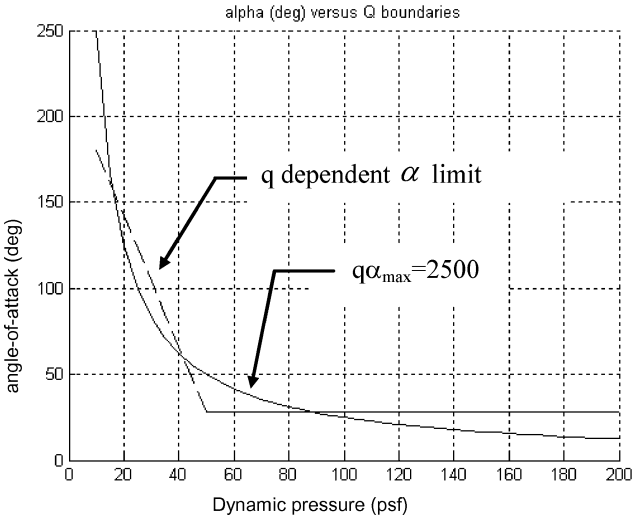

Fig. 5 Angle-of-attack constraint boundaries.

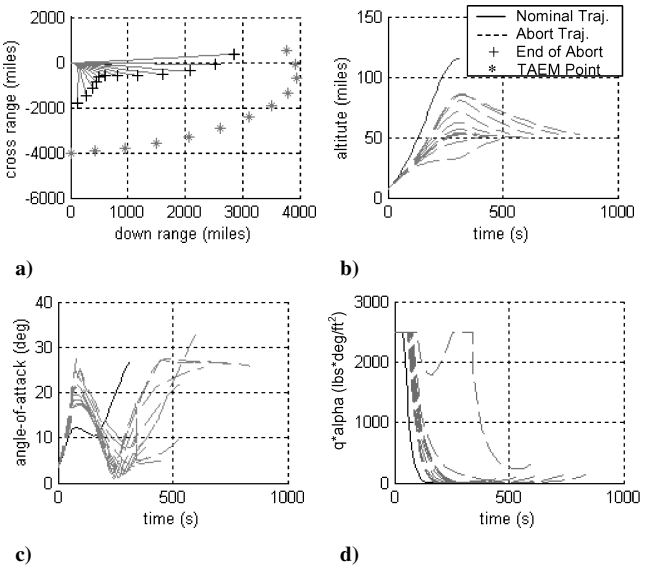

Fig. 6 Aborts to downrange TAEM points.

herein, $t = 0$ corresponds to the failure time. The structure of the abort maneuver after failure, in the sense of the number and times of boost and coast phases, depends on the TAEM point. The vehicle trajectory from the entry point up to the TAEM point is defined by a separate guidance algorithm.[13]

Figure 6 shows a set of abort trajectories for a range of TAEM points (each designated by an asterisk) downrange from the abort condition. The end of the abort trajectory, consisting of a boost phase followed by an atmospheric coast phase, is marked by plus symbols. The α limit is active for the cases with the largest cross range. The jumps in the angle-of-attack profiles occur at the start of the atmospheric coast stage. This is due to the discontinuity in thrust. From the altitude plot (Fig. 6b), it can be seen that aborts to the more downrange TAEM points reach higher altitudes than the aborts to the cross range points. Figure 7 shows the orbital conditions at the end of the abort trajectories and the duration of the atmospheric coast stages. The boost arc ends at 343.52 s in all of the abort cases due to the constraint on final mass. Figure 7a shows that most of the abort cases terminate near perigee, indicating that it is possible for the vehicle to attain an elliptical, or even slightly lower energy circular, orbit condition. Case number 0 in these results corresponds to the nominal ascent trajectory, and case number 10 is the abort trajectory with the largest negative cross range. Note from Fig. 8 that most of the abort trajectories, except for the last two cases, arrive at the terminal constraint set with excessive energy. [Dashed line is the linear fit of entry data as defined by Eq. (8).]

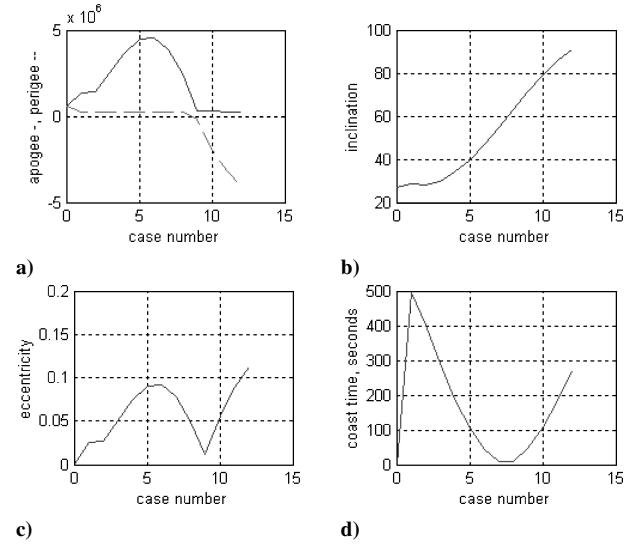

Fig. 7 Orbital parameters at end of the ascent for downrange aborts.

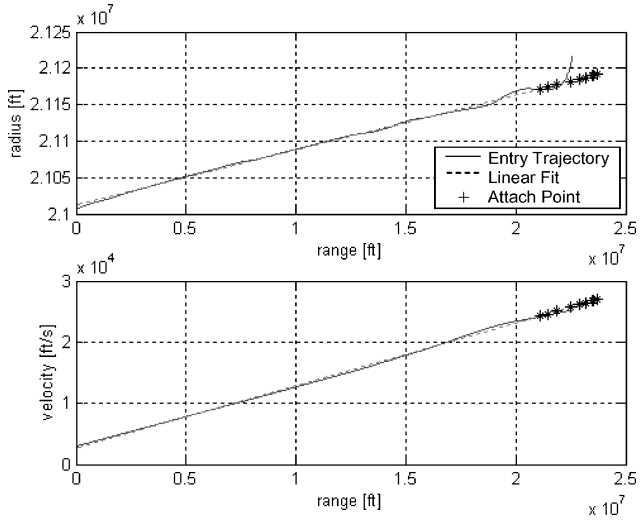

Fig. 8 Attachment to entry trajectory for downrange aborts.

There are a variety of approaches to avoid the problem of arriving at the terminal set with excessive energy. One is to burn less fuel during ascent and after entry dump the remaining amount. A second would be to turn off one of the operating engines while continuing to pump fuel through that engine. A third would be to delay the start of the abort trajectory. Solutions using these options attach to the entry trajectory at more reasonable energy values.[14]

For aborts forcing a return to the launch longitude, the depletion of energy during the initial turn prevents the vehicle from reaching the entry condition with excessive energy. Figure 9 shows solutions for a set of TAEM points located at the launch longitude. Both the $q \cdot \alpha$ and the α limits are active for portions of some of these solutions. Figure 10 shows that aborts to TAEM points farther away from the launch site contain atmospheric coast stages, but the last three cases do not. Also note that all of these cases end close to apogee and that there is a significant depletion of energy as the TAEM point is moved closer to the launch latitude. This loss of energy forces the vehicle to attach farther along the entry guidance path, as shown in Fig 11. Aborts to TAEM points close to the launch site are characterized by the use of large angles of attack, indicating a preference to pull up out of the atmosphere, where thrusting perpendicular to the velocity vector is used to accomplish the maneuver.

Attempts to find an abort solution to a TAEM point located closer to the launch site failed due to excessive loss in energy. Also, in the abort to down range cases, it was not possible to increase cross range beyond case 10 in Fig. 6. However, because entry guidance

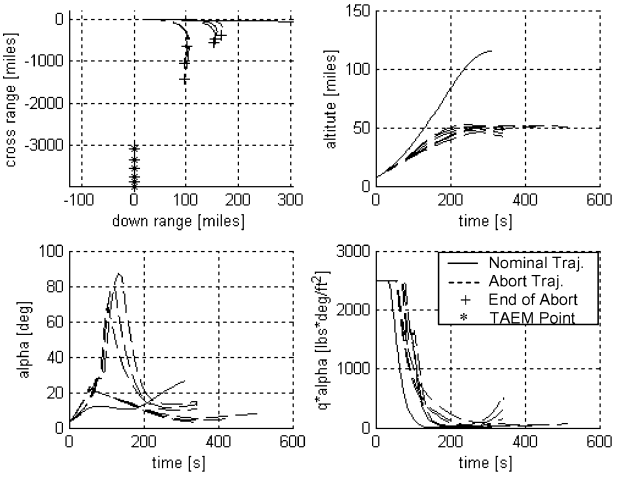

Fig. 9 Aborts to launch longitude TAEM points.

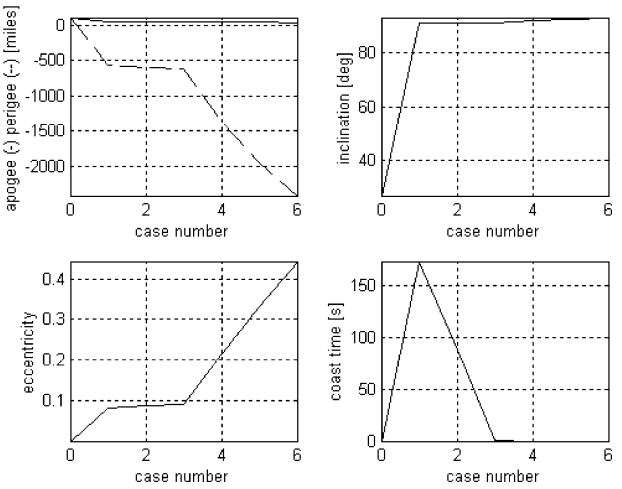

Fig. 10 Orbital parameters at end of ascent for return to launch longitude aborts.

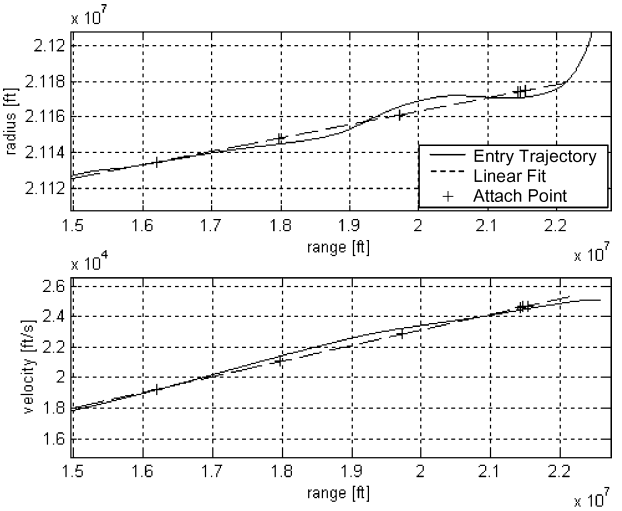

Fig. 11 Attachment to entry trajectory for return to launch longitude aborts.

can be used to perform a portion of the out-of-plane maneuvering, it may be possible to reach TAEM points located beyond this range of values.

The switching function for all of the downrange abort solutions, and for the nominal ascent trajectory, indicates that using maximum thrust in the abort is not an optimal strategy, especially for the more downrange cases. This suggests that examining a boost–coast–boost–coast solution would result in a solution with better

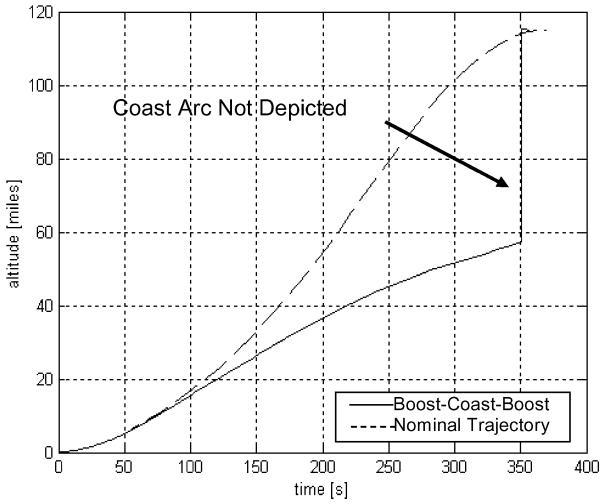

Fig. 12 Comparison of nominal ascent, boost vs boost–coast–boost.

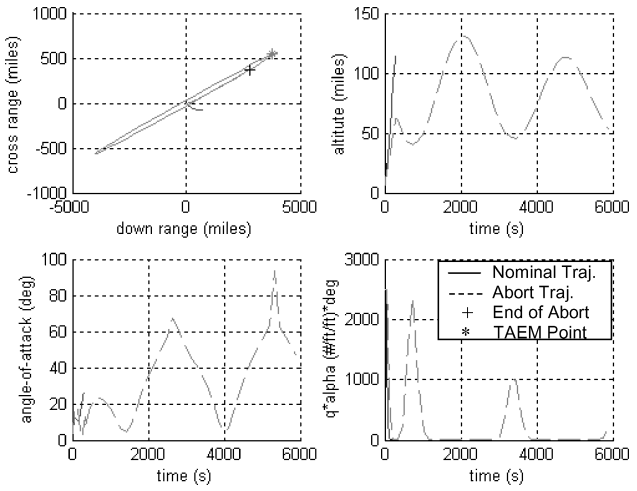

Fig. 13 Once-around abort trajectory.

performance. However, for aborts this would only be advisable if it is not possible to attain the terminal constraint set with a reasonable amount of energy. For nominal ascent, insertion of an optimized coast arc resulted in a fuel savings of 3022 lb. The resulting altitude profiles are shown in Fig. 12. In this case, only the boost time is shown on the horizontal axis.

The hybrid optimization method was also used to investigate the possibility of flying a once-around trajectory. A typical result is shown in Fig. 13. Note that these trajectories involve multiple skipping in and out of the atmosphere. This shows the usefulness of modeling atmospheric coast arcs, which are necessary to obtain a result of this type.

Convergence problems were experienced for the fixed-point iterative method used in the code to treat the collocation variables. This iteration is performed until the collocation values match the values calculated along the last computed trajectory. In many cases, particularly those involving turning back toward the launch longitude (significant aerodynamic maneuvering), it was necessary to relax the convergence criterion. At this point, it appears to be a major technical barrier to the methodology employed in the hybrid method. A detailed analysis has been carried out.[14] It is anticipated that when the guidance algorithm is implemented in closed form in an abort simulation this issue will not be as serious a problem as it first appears because the aerodynamic forces greatly decrease once the initial heading change is completed.

Conclusions

Modifications and extensions to a previously developed hybrid algorithm for future launch vehicle ascent trajectory optimization have been described. These changes allow for the generation of abort trajectories. A suitable terminal constraint set defining the entry conditions for the abort case has been derived. Transition to entry guidance is accomplished by attaching tangentially to the entry trajectory. It was found that aborts to downrange TAEM points arrive at the entry interface with excessive energy. Approaches to avoid this problem include delaying the start of the abort, leading to more reasonable energy levels. For aborts to launch longitude, there is a significant depletion of energy, depending on the entry guidance employed to reach these TAEM points. For nominal ascent and downrange aborts, a boost–coast–boost–coast solution results in significant fuel savings. A proof is provided that singular arcs are not feasible both in vacuum and during the atmospheric portion of the ascent.

Acknowledgments

This research was supported by the U.S. Air Force Research Laboratory/VACA Wright–Patterson under Contract F33615-00-C-3021 and by NASA Marshall Space Flight Center under Grant NAG3-1638. The authors express their appreciation to Gregory Dukeman of NASA Marshall Space Flight Center for discussions related to the theorem and its proof.

References

[1]Hanson, J., "Advanced Guidance and Control Project for Reusable Launch Vehicles," AIAA Paper 2000-3957, Aug. 2000.

[2]Calise, A. J., Melamed, N., and Lee, S., "Design and Evaluation of a Three-Dimensional Optimal Ascent Guidance Algorithm," *Journal of Guidance, Control, and Dynamics*, Vol. 21, No. 6, 1998, pp. 867–875.

[3]Gath, P. F., and Calise, A. J., "Optimization of Launch Vehicle Ascent Trajectories with Path Constraints and Coast Arcs," *Journal of Guidance, Control, and Dynamics*, Vol. 24, No. 2, 2001, pp. 296–304.

[4]Calise, A. J., Tandon, S., Young, D. H., and Kim, S., "Further Improvements to a Hybrid Method for Launch Vehicle Ascent Trajectory Optimization," AIAA Paper 2000-4261, Aug. 2000.

[5]Lu, P., Sun, H., and Tsai, B., "Closed-Loop Endoatmospheric Ascent Guidance," *Journal of Guidance, Control, and Dynamics*, Vol. 26, No. 2, 2003, pp. 283–294.

[6]Johnson, E. N., and Calise, A. J., "Reusable Launch Vehicle Adaptive Guidance and Control Using Neural Networks," AIAA Paper 2001-4381, Aug. 2001.

[7]Lawden, D. F., "Rocket Trajectory Optimization: 1950–1963," *Journal of Guidance, Control, and Dynamics*, Vol. 14, No. 4, 1991, pp. 705–711.

[8]Lawden, D. F., "Calculation of Singular Extremal Rocket Trajectories," *Journal of Guidance, Control, and Dynamics*, Vol. 15, No. 6, 1992, pp. 1361–1365.

[9]Robbins, H. M., "Optimality of Intermediate-Thrust Arcs of Rocket Trajectories," *AIAA Journal*, Vol. 3, No. 6, 1965, pp. 1094–1098.

[10]Goh, B. S., "The Second Variation for the Singular Bolza Problem," *SIAM Journal on Control and Optimization*, Vol. 4, No. 2, 1966, pp. 309–325.

[11]Jezewski, D. J., "Optimal Analytic Multiburn Trajectories," *AIAA Journal*, Vol. 10, No. 5, 1972, pp. 680–685.

[12]Mease, K. D., Chen, D. T., Teufel, P., and Schoenenberger, H., "Reduced-Order Entry Trajectory Planning for Acceleration Guidance," *Journal of Guidance, Control, and Dynamics*, Vol. 25, No. 2, 2002, pp. 257–266.

[13]Saraf, A., Leavitt, J. A., Chen, D. T., and Mease, K. D., "Design and Evaluation of an Acceleration Guidance Algorithm for Entry," *Journal of Spacecraft and Rockets* (to appear).

[14]Brandt, N., "Generation of Launch Vehicle Abort Trajectories Using a Hybrid Optimization Method," Diploma Thesis, Inst. of Flight Mechanics and Control, Univ. of Stuttgart, Stuttgart, Germany, May 2002.